nature materials

LETTERS

PUBLISHED ONLINE: 12 JANUARY 2014 | DOI: 10.1038/NMAT4181

Field-tunable spin-density-wave phases in $Sr_3Ru_2O_7$

C. Lester[1], S. Ramos[2], R. S. Perry[3], T. P. Croft[1], R. I. Bewley[4], T. Guidi[4], P. Manuel[4], D. D. Khalyavin[4], E. M. Forgan[5] and S. M. Hayden[1]*

The conduction electrons in a metal experience competing interactions with each other and the atomic nuclei. This competition can lead to many types of magnetic order in metals[1]. For example, in chromium[2] the electrons order to form a spin-density-wave (SDW) antiferromagnetic state. A magnetic field may be used to perturb or tune materials with delicately balanced electronic interactions. Here, we show that the application of a magnetic field can induce SDW magnetic order in a quasi-2D metamagnetic metal, where none exists in the absence of the field. We use magnetic neutron scattering to show that the application of a large ($B \approx 8$ T) magnetic field to the perovskite metal $Sr_3Ru_2O_7$ (refs 3–7) can be used to tune the material through two magnetically ordered SDW states. The ordered states exist over relatively small ranges in field ($\lesssim$0.4 T), suggesting that their origin is due to a new mechanism related to the electronic fine structure near the Fermi energy, possibly combined with the stabilizing effect of magnetic fluctuations[8,9]. The magnetic field direction is shown to control the SDW domain populations, which naturally explains the strong resistivity anisotropy or 'electronic nematic' behaviour observed[5,6] in this material.

The application of a magnetic field can profoundly effect the electrons in a solid, causing new ground states to form, such as the fractional quantum Hall state. Magnetic ground states can also be induced. For example, the Bechgaard salts, such as $(TMTSF)_2PF_6$, are quasi-1D metals that show a cascade of magnetic-field-induced SDW transitions[10–12]. Incommensurate magnetic order is induced inside the superconducting phase of the heavy fermion superconductor $CeCoIn_5$ (ref. 13) and also in certain insulating quantum magnets with anisotropic exchange interactions[14]. In this paper, we report the first observation of field-induced magnetic order in $Sr_3Ru_2O_7$. Interestingly, $Sr_3Ru_2O_7$ shares a common feature with Bechgaard salts[12] in that it has regions[5] of increased resistance ('plateaux' in the Bechgaard case) which are induced by the field.

$Sr_3Ru_2O_7$ is an itinerant metamagnet[15,16]—that is, a metal which undergoes a sudden change from a low- to high-magnetization state as a function of magnetic field. It has a layered perovskite structure (Fig. 1a) with conduction taking place in the RuO_2 bilayers. Thus, in contrast to the Bechgaard salts mentioned above, it has a quasi-2D electronic structure. For $\mathbf{B} \parallel \mathbf{c}$ (where $\mathbf{a}$, $\mathbf{b}$ and $\mathbf{c}$ are the crystallographic axes of Fig. 1a) and temperatures below $T \approx 1$ K, $Sr_3Ru_2O_7$ shows a rapid increase of magnetization[7] (Supplementary Fig. 2c) from 0.2 to 0.35 μ_B Ru^{-1} over a field range of about 1 T near the metamagnetic field, $B_c \approx 7.95$ T. The metamagnetic behaviour is believed to be caused[15–18] by proximity to ferromagnetism and the band structure having a local minimum in the density of states at the Fermi energy (ε_F) and/or a maximum near ε_F. Such features may result from a van Hove singularity near ε_F, as observed[19] by angle-resolved photo-emission spectroscopy.

A unique feature of $Sr_3Ru_2O_7$ is the observation of an unusual phase (denoted as 'A', see Fig. 2a) near B_c for $\mathbf{B} \parallel \mathbf{c}$ and for $T \lesssim 1$ K. The A-phase is a region of higher resistivity (Fig. 3b) whose boundaries can be identified from anomalies in a.c. susceptibility, resistivity, NMR and magnetostriction[5,20,21]. Tilting the field $\mathbf{B}$ away from $\mathbf{c}$ to give a component along $\mathbf{a}$ or $\mathbf{b}$ induces a large anisotropy ('electron nematic' behaviour) in the in-plane resistivity, both in the A-phase[6] and the adjacent region[22] in the B–T plane. For example, a $\mathbf{B}$ component along $\mathbf{a}$ causes $\mathbf{b}$ to become the easy direction for current flow (Fig. 3a–c). Related nematic behaviour has been observed in the iron-based superconductors (FeSCs), where it can be revealed by the application of uniaxial stress[23].

Motivated by previous reports[24,25] of strong low-energy spin fluctuations, we searched for static SDW order with higher energy resolution and lower temperatures. In SDW antiferromagnets the ordered moment is modulated in space with a wavevector $\mathbf{q}_{SDW}$. This results in satellite peaks at reciprocal space positions $\mathbf{Q} = \boldsymbol{\tau} + \mathbf{q}_{SDW}$, where $\boldsymbol{\tau}$ is a reciprocal lattice point (including $\boldsymbol{\tau} = (0, 0, 0)$) of the crystal structure. Fig. 1c shows Bragg scans along $\mathbf{Q} = (h, 0, 0)$ for a magnetic field $B_c = 7.95$ T and a series of temperatures in the range $0.05 < T < 1.2$ K which traverse the A-phase (Fig. 2a). Below $T \approx 1.0$ K, a magnetic Bragg peak develops at $\mathbf{q}^A_{SDW} = (0.233 \pm 0.002, 0, 0)$. Scans along other directions parallel to $\mathbf{b}^*$ and $\mathbf{c}^*$ (Supplementary Fig. 4) show that the peak is sharp in all three directions, indicating 3D magnetic ordering with in-plane correlation lengths greater than 350 Å. Energy-dependent scans through the ordering position (Supplementary Fig. 3) show that the peak is resolution limited in energy. This implies that the inverse lifetime of any magnetic fluctuations is less than $\tau^{-1} = 4$ μeV ≈ 40 mK ≈ 1 GHz. From the intensity of the Bragg peak we estimate the magnitude of the ordered moment (for $T = 50$ mK and $B = 7.95$ T) to be $\langle m_q \rangle = 0.10 \pm 0.02$ μ_B Ru^{-1}, assuming the structure in Fig. 4a. Figure 2b shows the intensity of the $\mathbf{q}^A_{SDW}$ Bragg peak measured as a function of magnetic field. We find that the onset of the Bragg peak coincides with the boundaries of the A-phase, indicating that it is associated with SDW order.

The susceptibility and resistivity (Fig. 3b) of $Sr_3Ru_2O_7$ show anomalous behaviour for fields above the A-phase boundary[5,6,22].

[1]H. H. Wills Physics Laboratory, University of Bristol, Bristol BS8 1TL, UK. [2]School of Physical Sciences, University of Kent, Canterbury CT2 7NH, UK. [3]London Centre for Nanotechnology and Department of Physics and Astronomy, University College London, London WC1E 6BT, UK. [4]ISIS Facility, Rutherford Appleton Laboratory, Chilton, Didcot OX11 0QX, UK. [5]School of Physics and Astronomy, University of Birmingham, Birmingham B15 2TT, UK. *e-mail: s.hayden@bristol.ac.uk

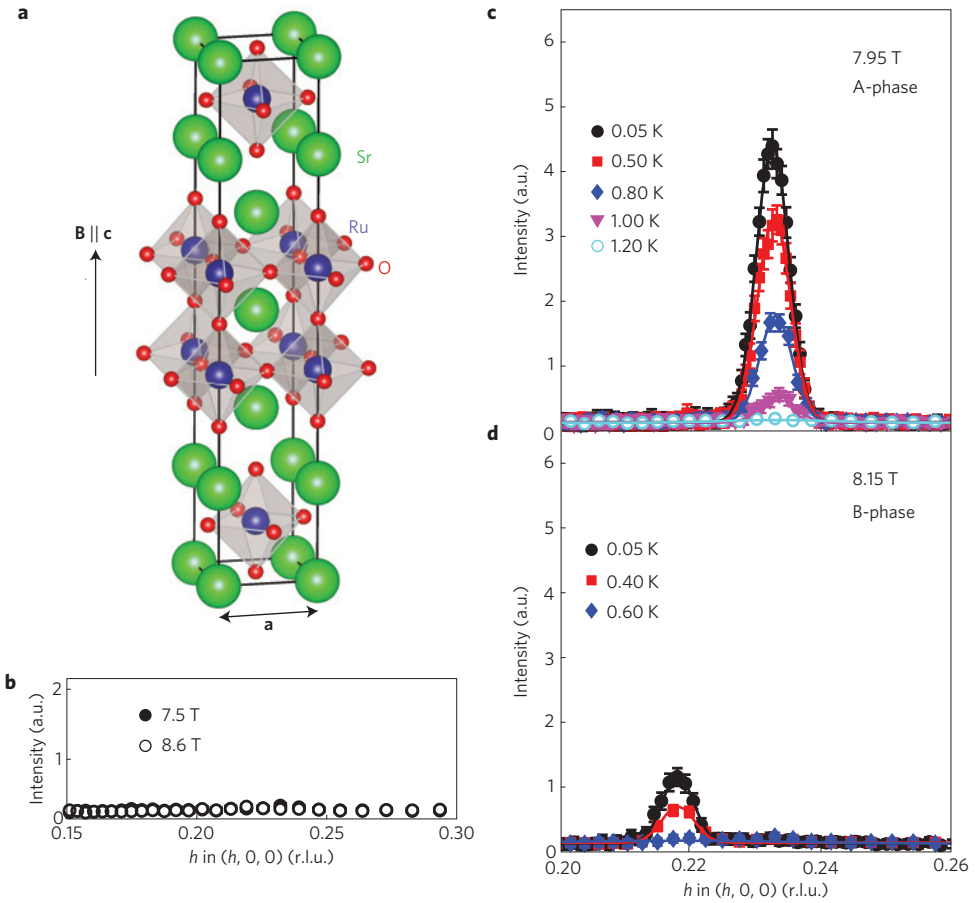

Figure 1 | Spin-density-wave order in $Sr_3Ru_2O_7$ observed by neutron diffraction. a, Tetragonal unit cell[32] of $Sr_3Ru_2O_7$ showing the direction of the applied field. We label reciprocal space, (h,k,l) in units of $(2\pi/a, 2\pi/b, 2\pi/c)$, based on this cell with $a=b=3.89$ Å and $c=20.7$ Å. **b**–**d**, Magnetic Bragg scattering data collected on the WISH spectrometer at various magnetic fields. **b**, $T=0.05$ K for $B=7.5$ and 8.6 T. **c**, $B=7.95$ T for $0.05\leq T\leq 1.20$ K. **d**, $B=8.15$ T for $0.05\leq T\leq 0.60$ K. SDW Bragg peaks are seen at $B=7.95$ T (A-phase, **c**) and 8.15 T (B-phase, **d**) with onset temperatures of 1 ± 0.05 and 0.5 ± 0.05 K, respectively. The SDW wavevector $\mathbf{q}_{SDW}$ changes discontinuously between the two phases. No SDW peaks are seen at $B=7.5$ or 8.6 T (**b**). Error bars are determined from the number of neutrons counted via Poisson statistics.

We therefore also searched for SDW order in this region. For fields greater than the upper boundary of the A-phase, we observe (Fig. 1d) an incommensurate peak at a different wavevector $\mathbf{q}^{B}_{SDW}=(0.218\pm0.002,0,0)$ to that observed in the A-phase. We denote this second SDW-ordered region the 'B-phase'.

The temperature and field dependencies of the $\mathbf{q}^{A}_{SDW}$ and $\mathbf{q}^{B}_{SDW}$ Bragg peak intensities are shown in Fig. 2b,c. For the $\mathbf{q}^{A}_{SDW}$ Bragg peak, we find that the fields and temperatures at which the magnetic order disappears coincide closely with the boundaries of the A-phase determined from a.c. susceptibility and resistivity[5]. The boundaries of the B-phase for $\mathbf{B}\parallel\mathbf{c}$ are less well characterized. A high-field tail to the resistivity anomaly is observed[6] for $8.1\lesssim B\lesssim 8.5$ T and $T=50$ mK, which defines the width of the B-phase in field. For a small tilt of the magnetic field away from the c-axis there is[22] a region of anisotropic resistance which persists up to 0.4 K and seems to correspond to the B-phase.

The SDW modulation of the ordered moment $[\mathbf{m}(\mathbf{r})]$ results in satellite peaks. For the body centred tetragonal lattice of $Sr_3Ru_2O_7$, we expect SDW peaks around the $\boldsymbol{\tau}=(0,0,0),(1,0,1),(0,1,1)$ and $(1,1,0)$ reciprocal lattice points (Fig. 4b). We observe satellite peaks along $(h,0,1)$, but not along $(0,k,1)$. The simplest structure consistent with this observation is the linear transverse SDW shown in Fig. 4a. Other structures such as a cycloid[8] with $\mathbf{m}(\mathbf{r})$ in the a–b plane or a modulation of the moment $\mathbf{m}(\mathbf{r})$ parallel to $\mathbf{c}$ would give satellite peaks along $(0,k,1)$ with similar intensity to those along $(h,0,1)$.

One of the most fascinating properties of the A-phase is its electron nematic behaviour[6]. For magnetic fields parallel to the c-axis, the A-phase is associated with a large increase in the resistivity ρ which is isotropic with respect to the direction of charge transport within the RuO_2 planes (Fig. 3b). By tilting the magnetic field away from the c-axis we can introduce an in-plane (IP) component of magnetic field $\mathbf{B}_{IP}$ along the a-axis. Under these conditions, charge transport in the A-phase becomes strongly anisotropic. For current parallel to the in-plane field and the a-axis, the resistance anomaly in $\rho_a(B)$ associated with the A-phase remains (Fig. 3b), whereas for currents perpendicular to $\mathbf{B}_{IP}$, the anomaly in $\rho_b(B)$ is completely suppressed (Fig. 3c).

We investigated the effect of similar tilted fields on the SDW order of the A-phase. For fields parallel to the c-axis (Fig. 3d) we observe two domains of the transverse SDW, one with a propagation vector $\mathbf{q}$ parallel to $\mathbf{a}^{\star}$ (giving peaks at $\pm0.233,0,0$) and the other with $\mathbf{q}$ parallel to $\mathbf{b}^{\star}$ (giving peaks at $0,\pm0.233,0$). When the field is tilted to give a component parallel to $\mathbf{a}$, the domain propagating along $\mathbf{b}$ is completely suppressed (Fig. 3e). Thus, the applied magnetic field allows fine control of domain populations and the presence of the SDW domain modulated along $\mathbf{a}$ (Fig. 3e) is associated with the resistance anomaly in ρ_a (Fig. 3c).

The existence of a SDW provides a natural explanation for the resistivity anomalies observed in $Sr_3Ru_2O_7$. SDW order in metals may increase the resistivity by gapping out the Fermi surface or by introducing additional scattering mechanisms due to the

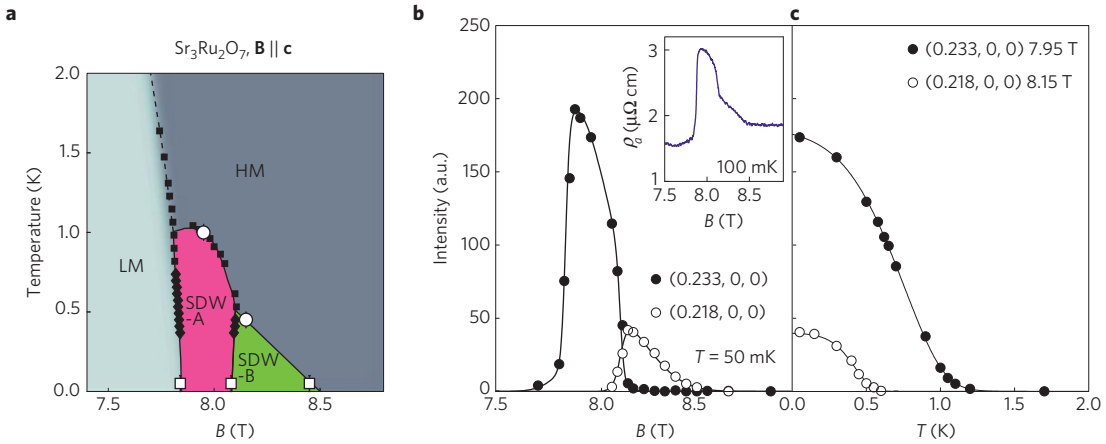

Figure 2 | Magnetic phase diagram of $Sr_3Ru_2O_7$. a, Phase diagram of $Sr_3Ru_2O_7$ determined from the present neutron scattering data combined with magnetic and transport measurements[5,6]. Dotted line represents the peak in χ separating low-moment (LM) and high-moment (HM) phases. Solid lines defining the A-phase boundaries are determined from maxima in χ, $d\rho/dB$ and $d^2\rho/dT^2$ (refs 5,6), and reproduced (Supplementary Fig. 2) on the present samples (filled diamonds and squares). SDW-A and SDW-B are SDW phases with different wavevectors. Open circles and squares respectively show the phase boundaries determined from the T and B dependence of Bragg peak intensities. The high-temperature boundary of SDW-B (solid line) is assumed to vary linearly with B. **b**,**c**, Magnetic field and temperature dependencies, respectively, of the $\mathbf{q}^{A}_{SDW}$ and $\mathbf{q}^{B}_{SDW}$ Bragg peak intensities. The inset to **b** shows the field-dependent resistivity $\rho_a(B)$ for a field parallel to the **c** direction[6]. The field varies by approximately 0.04 T over the sample, which may explain the apparent phase co-existence in **b**.

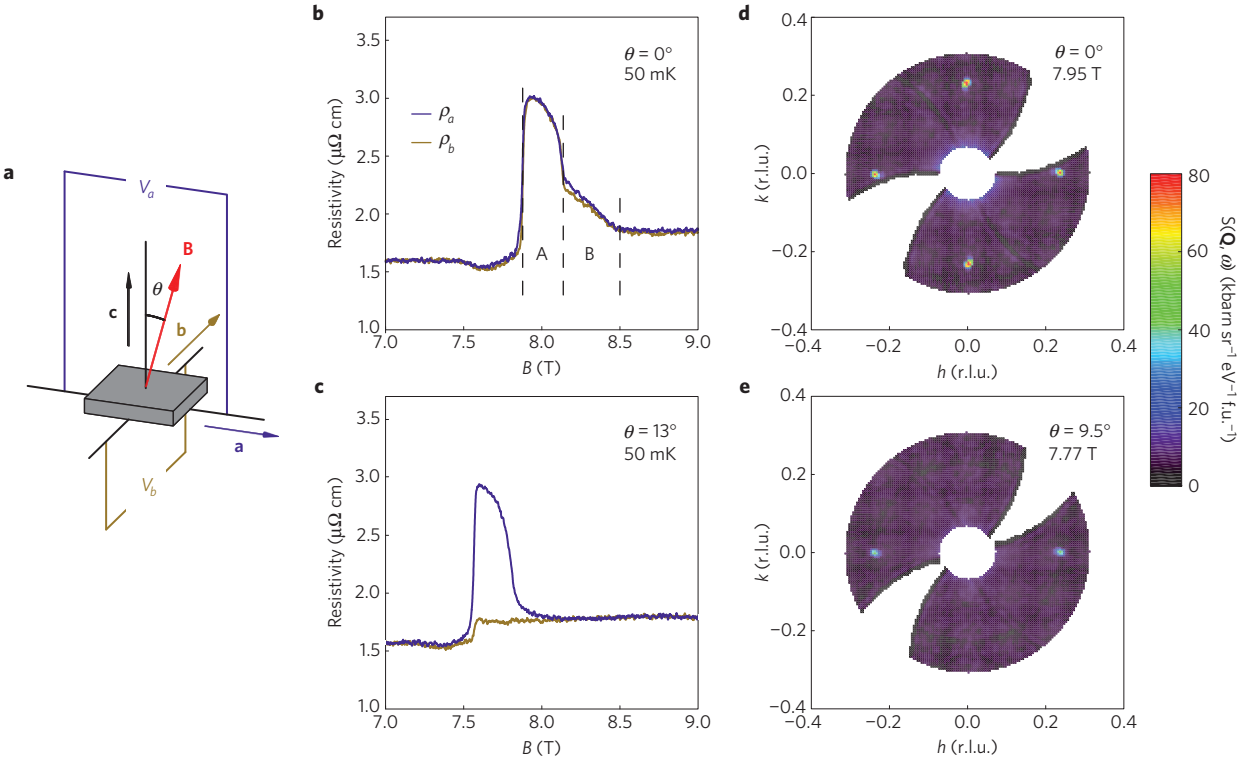

Figure 3 | The effect of tilting the magnetic field away from the *c*-axis on the SDW order and magnetoresistance. a–**c**, Anisotropic resistivity induced by tilted fields. For potentials V_a and V_b along the *a*- and *b*-axes and a magnetic field parallel to the crystalline *c*-axis, ρ_a and ρ_b are almost identical. **b**, An in-plane component of the field along the *a*-axis is created by tilting the magnetic field away from the *c*-axis and causes a marked reduction in ρ_b (ref. 6). **c**, At $\theta = 13°$, the SDW B-phase is suppressed[6]. **d**,**e**, Elastic (Bragg) scattering for $T = 50$ mK. Data are integrated over $-0.1 < l < 0.1$ r.l.u. and $-15 < E < 15$ μeV. For fields parallel to the *c*-axis (**d**), four Bragg satellites are seen corresponding to two SDW domains with wavevectors parallel to $\mathbf{a}^\star$ and $\mathbf{b}^\star$. Tilting the field to give a component along the *a*-axis (**e**) suppresses the SDW domain propagating along $\mathbf{b}^\star$. The large increase in resistivity shown in **b** and **c** is caused by a SDW with a propagation vector parallel to the current flow.

excitations associated with the magnetic order[2]. For example, the Bechgaard salts[12] show plateaux of increased resistance as a function of field where SDW order occurs, and the FeSC parent compound $BaFe_2As_2$ shows a peak[23] at its Néel temperature. For $Sr_3Ru_2O_7$, the field-dependent resistivity shown in Fig. 3b closely tracks the sum of the two magnetic order parameters (as measured by the SDW Bragg peak intensities) for the A and B phases (Fig. 2b). The gapping of the Fermi surface will be closely related to the SDW order parameter,

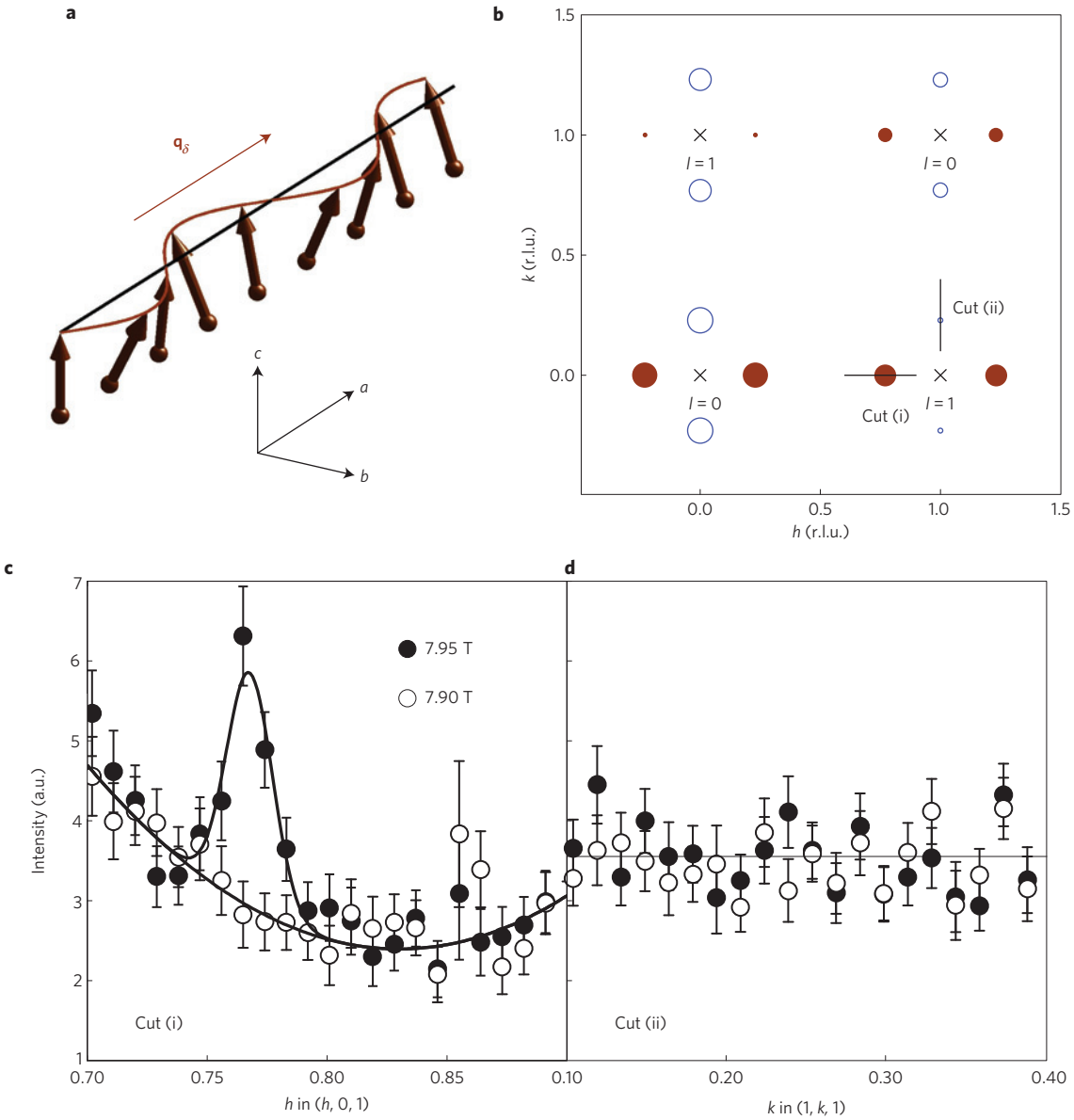

Figure 4 | The structure of the SDW. a, Proposed structure of a single domain of the SDW A-phase (**B** ∥ **c**) in $Sr_3Ru_2O_7$, a transverse spin density wave with $\mathbf{q}_{SDW} = (\delta, 0, 0)$. Arrows represent moments on the Ru sites of Fig. 1a. **b**, The SDW domain in **a** gives rise to satellite peaks (filled circles) at $\mathbf{Q} = \boldsymbol{\tau} \pm \mathbf{q}_{SDW}$. Crosses denote the positions of the parent reciprocal lattice positions ($\boldsymbol{\tau}$). Open circles are peaks associated with the domain with $\mathbf{q}_{SDW} = (0, \delta, 0)$. The areas of the circles represent the intensities of the satellite Bragg peaks for the structure in **a**. **c**, Elastic data collected using the LET spectrometer along cut (i) in **b**, showing a SDW Bragg peak. **d**, Data collected along cut (ii) in **b**, showing a SDW peak with zero or small intensity, consistent with the structure in **a**. The intensity is proportional to the square of the component of $\mathbf{m}_\mathbf{q}$ perpendicular to **Q**. The difference in the intensities of the two cuts arises from the direction of **m**(**r**) in **a** and not from the different populations of the two SDW domains. Error bars are determined from the number of neutrons counted via Poisson statistics.

hence we believe the removal of electronic states from near the Fermi surface is the most likely cause of the resistivity anomalies.

The formation of SDWs in metals (for example, Cr) is usually described in terms of a Stoner theory including a wavevector-dependent susceptibility $\chi_0(\mathbf{q})$ and an exchange interaction parameter I (refs 1,2). SDW order occurs when the generalized Stoner criterion $\chi_0(\mathbf{q})I \geq 1$ is satisfied. The ordering wavevector $\mathbf{q}_{SDW}$ is determined from the peak in $\chi_0(\mathbf{q})$, and ultimately by Fermi surface nesting. In the vicinity of a metamagnetic transition, the Fermi surface changes rapidly with field as the Fermi energy of one of the spin species passes through a peak in the density of states. Such a rapid change may lead to a SDW phase that is favoured over only a narrow range in field[26]. In $Sr_3Ru_2O_7$, two slightly different SDW states can be favoured. We note that the α_1 and γ_3 sheets[19] provide approximately the right nesting vectors to match $\mathbf{q}^{A}_{SDW}$ and $\mathbf{q}^{B}_{SDW}$ (refs 19,24,27). It has recently been proposed[8,9]—based on a microscopic Stoner theory and a Landau–Ginzburg expansion—that transverse spin modulated states can be further stabilized by soft transverse magnetic fluctuations[15,16].

The linear transverse nature of the SDW is not obviously predicted by the Landau–Ginzburg theory[8,9]. However, linearly polarized SDWs such as the one observed here (also in metals such as Cr, ref. 2) may be favoured by additional contributions[28,29] to the free energy. In the absence of strong anisotropy, antiferromagnets usually favour $\mathbf{m}_\mathbf{q} \perp \mathbf{B}$ and hence favour the structure for the A-phase shown in Fig. 4a. This structure would naturally host single-**q** domains. These would be enhanced or suppressed by tilting the field away from **c**, leading to the population imbalance shown in

Fig. 3e. The imbalance naturally explains the observed 'nematic' (anisotropic) transport properties of the SDW A-phase.

It is interesting to compare $Sr_3Ru_2O_7$ with iron-based superconductors. For current directions in the Fe–As planes, these materials (for example, $Ba(Fe_{1-x}Co_x)_2As_2$) show an anisotropic resistivity (nematic behaviour) which is associated with antiferromagnetism (AF) or its formation[23]. In contrast with $Sr_3Ru_2O_7$, the resistivity in the direction parallel to the propagation vector of the AF order is smallest[23]. The implication here is that there is more than one route to electronic nematic behaviour. The antiferromagnetism and nematic behaviour can be controlled very effectively by the use of uniaxial pressure or lattice strain[23] in the FeSCs. The application of an in-plane magnetic field[30] to $Ba(Fe_{1-x}Co_x)_2As_2$ causes a partial detwinning of the crystal and induces a strain field which can couple to the nematic susceptibility, yielding anisotropic transport properties. This contrasts with $Sr_3Ru_2O_7$, where an in-plane magnetic field induces anisotropy through the electronic effect described in this paper.

As mentioned above there are other examples of magnetic-field-induced incommensurately modulated states. The quasi-1D organic metallic Bechgaard salts show a cascade of magnetic-field-induced SDW transitions[10]. This is caused by the effect on the spin susceptibility[11] of the orbital motion of electrons in open orbits and leads to a series of phases spaced evenly in $1/B$. We believe that the quasi-2D nature of the band structure in $Sr_3Ru_2O_7$ results in a different mechanism. Another case is the heavy fermion superconductor $CeCoIn_5$ (ref. 13). Here a 'Q-phase' with spatially modulated superconducting and magnetic order parameters is created abutting B_{c2}. This spin modulation is associated with the superconductivity. Finally, the application of a magnetic field to certain insulating quantum magnets with anisotropic magnetic interactions, such as $TlCuCl_3$, can cause a Bose–Einstein condensation of magnons and antiferromagnetic order[14].

We observe SDW order in $Sr_3Ru_2O_7$ and show that the order parameter correlates strongly with the electronic nematic properties of the compound. This suggests that the SDW is at the root of the electronic nematic behaviour for this system. $Sr_3Ru_2O_7$ initially attracted attention because it exhibited signatures[31] of quantum criticality near B_c. The observation of SDW order provides a natural order parameter to associate with this quantum criticality and a basis for understanding the associated physical properties. One can ask whether other examples of field-induced SDWs can be found in quasi-2D metals and what conditions are required for their existence. The relevant special properties of $Sr_3Ru_2O_7$ may include its nested Fermi surface, the existence of a van Hove singularity near the Fermi energy and the concomitant metamagnetic transition, and its strongly enhanced magnetic susceptibility.

Methods

Single crystals of $Sr_3Ru_2O_7$ were grown using an image furnace method. Resistivity and magnetization measurements (Supplementary Fig. 1) were used to confirm sample quality was comparable to that of samples used in other studies[5–7]. The residual resistivity extrapolated to zero temperature of all samples was found to be less than 1 μΩcm. SQUID magnetometry, measured down to 2 K, found no evidence for the presence of ferromagnetic minority phases. To verify the presence of the anomalous phase (referred to as SDW-A in main text) in our samples we made low-temperature measurements of the a.c. susceptibility $\chi_{a.c.}$. By measuring $\chi_{a.c.}$ as a function of temperature and field, we were able to reproduce the phase diagram shown in Fig. 2a (Supplementary Fig. 2).

We used the LET spectrometer and WISH diffractometer at the ISIS spallation source in the UK to make our neutron scattering measurements. The LET spectrometer uses a monochromatic direct-geometry time-of-flight technique with position-sensitive detectors and the data in Fig. 3 were collected with an incident energy $E_i = 0.75$ meV. WISH is a white-beam instrument on a solid methane moderator and the Bragg peaks measured in Figs 1, 2 and 4 correspond to an incident energy of 3.5 meV. The samples were mounted in high-field magnet systems with He-3/He-4 dilution inserts. We used an aligned array of crystals with total mass 6.6 g for the LET experiment and a single crystal of mass 0.8 g for the WISH experiment. The data were collected with $\mathbf{B}$ vertical, $\mathbf{k}_i$ horizontal and $\mathbf{c}^*$ vertical or tilted as described in the text. Our LET data have been placed on an absolute scale by comparing the count rate from the sample with that from a plate of vanadium.

Neutron data are transformed from time-of-flight and angle to reciprocal space and energy. We have labelled reciprocal space as $\mathbf{Q} = h\mathbf{a}^* + k\mathbf{b}^* + \ell\mathbf{c}^*$, where $|\mathbf{a}^*| = 2\pi/a$ and so on, based on the simple tetragonal unit cell with $a = 3.89$ Å and $c = 20.7$ Å. The error bars in the raw data shown are determined from the total counts using Poisson statistics. We estimate the size of the ordered moment from the scattered neutron intensity[1],

$$\frac{\mathrm{d}^2\sigma}{\mathrm{d}\Omega\,\mathrm{d}E} = \frac{|\mathbf{k}_f|}{|\mathbf{k}_i|}\frac{1}{\mu_B^2}\left(\frac{\gamma r_e}{2}\right)^2 |F(\mathbf{Q})|^2\, C_{\mathbf{M}^\perp,\mathbf{M}^\perp}(\mathbf{q},\omega)$$

where $\mathbf{M}^\perp(\mathbf{r},t)$ is the moment perpendicular to the scattering vector $\mathbf{Q} = \mathbf{k}_i - \mathbf{k}_f$, $C(\mathbf{q},\omega)$ is the power spectrum of the magnetic correlations (including any ordered moment), γ is the gyromagnetic ratio of the neutron, r_e is the classical electron radius, and $|F(\mathbf{Q})|^2$ is the magnetic form factor. Throughout the text we have expressed the local moment as $\mathbf{M}(\mathbf{r}) = \mathbf{M} + \mathbf{m}(\mathbf{r})$, where $\mathbf{M}$ is the ferromagnetic moment induced by the field and $\mathbf{m}(\mathbf{r})$ is the spatially varying moment due to the SDW. To obtain the integrated intensity of the SDW-A Bragg peak, we integrated over the ranges $\Delta h = 0.01$, $\Delta k = 0.02$, $\Delta l = 0.2$ and $\Delta E = 0.015$ meV. We assumed the magnetic structure in Fig. 4a and that each SDW domain occupied 50% of the sample. We integrated a single peak and multiplied this moment by four to obtain the value for the full Brillouin zone (that is per two Ru atoms). The value quoted in the main text is per Ru.

Received 17 September 2014; accepted 21 November 2014; published online 12 January 2014

References

1. White, R. M. *Quantum Theory of Magnetism* (Springer, 2007).
2. Fawcett, E. Spin-density-wave antiferromagnetism in chromium. *Rev. Mod. Phys.* **60,** 209–283 (1988).
3. Ikeda, S-I., Maeno, Y., Nakatsuji, S., Kosaka, M. & Uwatoko, Y. Ground state in $Sr_3Ru_2O_7$ Fermi liquid close to a ferromagnetic instability. *Phys. Rev. B* **62,** R6089–R6092 (2000).
4. Perry, R. S. *et al.* Metamagnetism and critical fluctuations in high quality single crystals of the bilayer ruthenate $Sr_3Ru_2O_7$. *Phys. Rev. Lett.* **86,** 2661–2664 (2001).
5. Grigera, S. A. *et al.* Disorder-sensitive phase formation linked to metamagnetic quantum criticality. *Science* **306,** 1154–1157 (2004).
6. Borzi, R. A. *et al.* Formation of a nematic fluid at high fields in $Sr_3Ru_2O_7$. *Science* **315,** 214–217 (2007).
7. Rost, A. W., Perry, R. S., Mercure, J. F., Mackenzie, A. P. & Grigera, S. A. Entropy landscape of phase formation associated with quantum criticality in $Sr_3Ru_2O_7$. *Science* **325,** 1360–1363 (2009).
8. Berridge, A. M., Green, A. G., Grigera, S. A. & Simons, B. D. Inhomogeneous magnetic phases: A Fulde–Ferrell–Larkin–Ovchinnikov-like phase in $Sr_3Ru_2O_7$. *Phys. Rev. Lett.* **102,** 136404 (2009).
9. Conduit, G. J., Green, A. G. & Simons, B. D. Inhomogeneous phase formation on the border of itinerant ferromagnetism. *Phys. Rev. Lett.* **103,** 207201 (2009).
10. Kwak, J. F., Schirber, J. E., Greene, R. L. & Engler, E. M. Magnetic quantum oscillations in tetramethyltetraselenafulvalenium hexafluorophosphate $[(TMTSF)_2PF_6]$. *Phys. Rev. Lett.* **46,** 1296–1299 (1981).
11. Gorkov, L. P. & Lebed, A. G. On the stability of the quasi-one-dimensional metallic phase in magnetic fields against the spin density wave formation. *J. Phys. Lett.* **45,** L433 (1984).
12. Chaikin, P. M., Chashechkina, E. I., Lee, I. J. & Naughton, M. J. Field-induced electronic phase transitions in high magnetic fields. *J. Phys. Condens. Matter* **10,** 11301–11314 (1998).
13. Kenzelmann, M. *et al.* Coupled superconducting and magnetic order in $CeCoIn_5$. *Science* **321,** 1652–1654 (2008).
14. Zapf, V., Jaime, M. & Batista, C. D. Bose–Einstein condensation in quantum magnets. *Rev. Mod. Phys.* **86,** 563–614 (2014).
15. Wohlfarth, E. P. & Rhodes, P. Collective electron metamagnetism. *Phil. Mag.* **7,** 1817–1824 (1962).
16. Shimizu, M. Itinerant electron metamagnetism. *J. Phys.* **43,** 155–163 (1982).
17. Millis, A. J., Schofield, A. J., Lonzarich, G. G. & Grigera, S. A. Metamagnetic quantum criticality in metals. *Phys. Rev. Lett.* **88,** 217204 (2002).
18. Binz, B. & Sigrist, M. Metamagnetism of itinerant electrons in multi-layer ruthenates. *Europhys. Lett.* **65,** 816–822 (2004).
19. Tamai, A. *et al.* Fermi surface and van Hove singularities in the itinerant metamagnet $Sr_3Ru_2O_7$. *Phys. Rev. Lett.* **101,** 026407 (2008).
20. Kitagawa, K. *et al.* Metamagnetic quantum criticality revealed by ^{17}O-NMR in the itinerant metamagnet $Sr_3Ru_2O_7$. *Phys. Rev. Lett.* **95,** 127001 (2005).
21. Stingl, C., Perry, R. S., Maeno, Y. & Gegenwart, P. Symmetry-breaking lattice distortion in $Sr_3Ru_2O_7$. *Phys. Rev. Lett.* **107,** 026404 (2011).

22. Bruin, J. A. N. *et al.* Study of the electronic nematic phase of $Sr_3Ru_2O_7$ with precise control of the applied magnetic field vector. *Phys. Rev. B* **87,** 161106 (2013).
23. Chu, J-H. *et al.* In-plane resistivity anisotropy in an underdoped iron arsenide superconductor. *Science* **329,** 824–826 (2010).
24. Capogna, L. *et al.* Observation of two-dimensional spin fluctuations in the bilayer ruthenate $Sr_3Ru_2O_7$ by inelastic neutron scattering. *Phys. Rev. B* **67,** 012504 (2003).
25. Ramos, S. *et al.* Spin dynamics in $Sr_3Ru_2O_7$ near the metamagnetic transition by inelastic neutron scattering. *Physica B* **403,** 1270–1272 (2008).
26. Rice, T. M. Band-structure effects in itinerant antiferromagnetism. *Phys. Rev. B* **2,** 3619–3630 (1970).
27. Singh, D. J. & Mazin, I. I. Electronic structure and magnetism of $Sr_3Ru_2O_7$. *Phys. Rev. B* **63,** 165101 (2001).
28. Overhauser, A. W. Spin density waves in an electron gas. *Phys. Rev.* **128,** 1437–1452 (1962).
29. Walker, M. B. Phenomenological theory of the spin-density-wave state of chromium. *Phys. Rev. B* **22,** 1338–1347 (1980).
30. Chu, J-H. *et al.* In-plane electronic anisotropy in underdoped $Ba(Fe_{1-x}Co_x)_2As_2$ revealed by partial detwinning in a magnetic field. *Phys. Rev. B* **81,** 214502 (2010).
31. Grigera, S. A. *et al.* Magnetic field-tuned quantum criticality in the metallic ruthenate $Sr_3Ru_2O_7$. *Science* **294,** 329–332 (2001).
32. Shaked, H., Jorgensen, J., Chmaissem, O., Ikeda, S. & Maeno, Y. Neutron diffraction study of the structural distortions in $Sr_3Ru_2O_7$. *J. Solid State Chem.* **154,** 361–367 (2000).

Acknowledgements

We acknowledge helpful discussions with A. P. Mackenzie, R. Coldea, Y. Maeno, R. Evans and R. M. Richardson. We are grateful to S. A. Grigera and A. P. Mackenzie for providing resistivity data from ref. 6 which is reproduced in Figs 2 and 3. Our work was supported by the UK EPSRC (Grant No. EP/J015423/1).

Author contributions

C.L. and R.S.P. prepared the samples. All authors planned and made the neutron scattering measurements. C.L. and S.M.H. analysed the data and wrote the manuscript. All authors contributed to the discussion and provided input to the manuscript.

Additional information

Supplementary information is available in the online version of the paper. Reprints and permissions information is available online at www.nature.com/reprints. Correspondence and requests for materials should be addressed to S.M.H.

Competing financial interests

The authors declare no competing financial interests.